

All carbon p-n border in bilayer graphene by the molecular orientation of intercalated corannulene

Cite as: J. Appl. Phys. **131**, 134303 (2022); <https://doi.org/10.1063/5.0083616>

Submitted: 28 December 2021 • Accepted: 17 March 2022 • Published Online: 05 April 2022

 Mina Maruyama and  Susumu Okada



View Online



Export Citation



CrossMark

ARTICLES YOU MAY BE INTERESTED IN

Stochastic behavior of an interface-based memristive device


Journal of Applied Physics **131**, 134304 (2022); <https://doi.org/10.1063/5.0084085>

Impact of mobility degradation on endurance fatigue of FeFET with TiN/Hf_{0.5}Zr_{0.5}O₂/SiO_x/Si (MFIS) gate structure


Journal of Applied Physics **131**, 134102 (2022); <https://doi.org/10.1063/5.0084816>

Electron g-factor determined for quantum dot circuit fabricated from (110)-oriented GaAs quantum well

Journal of Applied Physics **131**, 134305 (2022); <https://doi.org/10.1063/5.0086555>



HIDEN
ANALYTICAL



40
YEARS
1982-2022


Instruments for Advanced Science

- Knowledge,
- Experience,
- Expertise

Click to view our product catalogue


Contact Hiden Analytical for further details:
www.HidenAnalytical.com
info@hideninc.com

Gas Analysis




- ▶ dynamic measurement of reaction gas streams
- ▶ catalysis and thermal analysis
- ▶ molecular beam studies
- ▶ dissolved species probes
- ▶ fermentation, environmental and ecological studies

Surface Science




- ▶ UHVTPD
- ▶ SIMS
- ▶ end point detection in ion beam etch
- ▶ elemental imaging - surface mapping

Plasma Diagnostics



- ▶ plasma source characterization
- ▶ etch and deposition process reaction kinetic studies
- ▶ analysis of neutral and radical species

Vacuum Analysis



- ▶ partial pressure measurement and control of process gases
- ▶ reactive sputter process control
- ▶ vacuum diagnostics
- ▶ vacuum coating process monitoring

All carbon p-n border in bilayer graphene by the molecular orientation of intercalated corannulene

Cite as: J. Appl. Phys. **131**, 134303 (2022); doi: [10.1063/5.0083616](https://doi.org/10.1063/5.0083616)

Submitted: 28 December 2021 · Accepted: 17 March 2022 ·

Published Online: 5 April 2022



Mina Maruyama^{a)} and Susumu Okada^{b)}

AFFILIATIONS

Department of Physics, Graduate School of Pure and Applied Sciences, University of Tsukuba, 1-1-1 Tennodai, Tsukuba, Ibaraki 305-8571, Japan

^{a)}Author to whom correspondence should be addressed: mmaruyama@comas-tsukuba.jp

^{b)}E-mail: sokada@comas-tsukuba.jp

ABSTRACT

Geometric and electronic structures of a corannulene ($C_{20}H_{10}$) intercalated bilayer graphene are investigated in terms of the molecular conformation using density functional theory. Our calculations indicate that the electronic structure of bilayer graphene is tunable by controlling the molecular conformation of corannulene. Holes and electrons coexist on the upper and lower layers of graphene, which are situated at the convex region and edge of corannulene when it has the bowl conformation. In contrast, bilayer graphene has a tiny gap of 4.7 meV at the K point owing to the substantial interaction between graphene and corannulene when corannulene has flat conformation. Electron and hole redistribution in bilayer graphene intercalating corannulene indicated the possibility of all carbon p-n border at an interface between corannulene with convex and concave arrangements. The intercalation substantially decreases the energy difference between the ground state bowl conformation and the metastable state flat conformation by approximately 400 meV. Accordingly, the two-dimensional nano-spacing between the graphene layers changes the molecular conformation of corannulene from a bowl to a flat structure at 139 MPa.

Published under an exclusive license by AIP Publishing. <https://doi.org/10.1063/5.0083616>

I. INTRODUCTION

Graphite has attracted much attention in pure and applied sciences over the last century because it is a common elemental condensed matter possessing exotic physical and chemical properties.^{1,2} Graphite has constituent layers called graphene, which has unique mechanical, thermal, optical, and electronic properties.^{3–6} The honeycomb covalent network of σ bonds of sp^2 C atoms in graphene endows it with remarkable mechanical stiffness⁴ and high thermal conductivity.⁵ Itinerant π electrons in this honeycomb network cause further unique physical and chemical properties such as conical dispersion bands at the Fermi level and at the six corners of the two-dimensional Brillouin zone. This conical dispersion band with its network topology gives graphene a remarkable carrier mobility of a few hundred thousand $cm^2 V^{-1} s^{-1}$ (Refs. 7–10) and peculiar electron states when appropriate boundary conditions are imposed.^{11–14} In contrast, owing to the weak dispersive interaction between graphene layers, graphite has thermal and electronic transport between layers that is an order of magnitude lower than along a sheet. The weak dispersive interlayer interaction allows us to tailor the mutual stacking arrangement of graphene layers. Although

natural graphite possesses Bernal (AB) or rhombohedral (ABC) interlayer stacking, twisted bilayer and few layer graphene have been synthesized as turbostratic graphite thin films where the twisting angle is precisely controllable.^{15–18} In such systems, wave function hybridization between layers causes versatile electronic properties depending on the stacking arrangement and the number of graphene layers.^{19,20} The surface of rhombohedral graphite exhibits spin polarization owing to the edge localized mode arising from the symmetry breaking of the sublattice structure across layers,^{21,22} and superconductivity has been observed on twisted bilayer graphene with a particularly small twisting angle.²³

Graphite is also an important host material for intercalation compounds with various guest atoms and molecules, owing to stable two-dimensional covalent networks that are bound via weak interaction with a 0.3 nm vacuum spacing. These compounds are called graphite intercalation compounds (GICs).^{2,24} GICs have a wide variety of physical properties that strongly depend on the guest intercalants. Depending on the stoichiometry and staged structure, intercalation of alkaline and alkaline-earth elements enhances the transport properties of GICs^{25–28} through charge

transfer from these atoms to graphite and hybridization between their electron states.^{29,30} Magnetism has also been induced by intercalated atoms or molecules with spin polarization.³¹ In addition to atomic intercalants, molecules and fullerene materials such as aromatic hydrocarbon molecules and fullerenes can be accommodated in interlayer spaces of graphite.^{32–37} Guest materials form two-dimensional layered structures in nanoscale spacing between graphene layers, where the intercalant materials possess different arrangements from their bulk forms.

Recent advances in layer-by-layer growth techniques for graphene and other atomic layered materials such as h-BN and transition-metal dichalcogenides^{15–17} have yielded a new class of GICs called van der Waals heteromaterials, where both the host graphene and guest materials form two-dimensional covalent networks. Layer-by-layer growth also has the potential to produce unique GICs where unusual molecules are intercalated in interlayer spacings of graphite or graphene thin films. Furthermore, the technique can control the GIC thickness, leading to bilayer graphene intercalating with atoms or molecules as ultimate versions of GICs.^{38,39} Buckybowls such as corannulene ($C_{20}H_{10}$)^{40,41} and sumanene ($C_{21}H_{12}$)⁴² are plausible intercalant molecules for bilayer graphene that may yield unusual physical and chemical properties because these molecules can form a two-dimensional triangular lattice on appropriate substrates^{43–45} and a substantial dipole moment normal to the molecular plane. The electronic structure of bilayer graphene is expected to be modulated by the intercalations of the buckybowls.⁴⁶ Their conformations and arrangements are also expected to be different from those in the bulk condensed phases of corannulene and sumanene in carbon nanotubes.⁴⁷

In this work, we investigate the physical properties of corannulene-intercalated bilayer graphene using density functional theory (DFT).^{48,49} Confined nanoscale spacing between the graphene layers and substantial interaction may enhance modulation of the molecular conformation or arrangement in bilayer graphene because corannulene undergoes inversion structural modulation via flat transition conformation. Our calculations reveal that a graphene layer

substantially decreases the energy barrier of the bowl-inversion reaction by approximately 0.4 eV, making the flat transition conformation stable with an energy being close to that of the bowl conformation. We also demonstrate that the two-dimensional nano-spacing between the graphene layers changes the molecular conformation of corannulene from bowl to flat under a compression of 139 MPa. Owing to the dipole moment arising from its bowl shape, corannulene intercalated in bilayer graphene induces a charge transfer between the graphene layers owing to the electron polarization in the molecule. Holes and electrons, each with a density of $5.3 \times 10^{12}/\text{cm}^2$, are induced on graphene layers located at the convex and edge sides of corannulene, respectively. Therefore, corannulene-intercalated bilayer graphene has potential application in semiconducting devices where the material itself works as p-n border at the interface where the intercalation compound possesses a different corannulene arrangement.

II. CALCULATION METHOD

The geometric and electronic structures of corannulene-intercalated bilayer graphene were investigated using the STATE package based on DFT.^{50,51} For the exchange-correlation potential energy among interacting electrons, the generalized gradient approximation was used with the Perdew–Burke–Ernzerhof functional forms.^{52,53} The dispersive interaction between corannulene and graphene was treated using vdW-DF2 with the C09 exchange-correlation functional.^{54–56} An ultrasoft pseudopotential was used to describe electron–ion interactions.⁵⁷ A plane-wave basis set with cutoff energies of 25 and 225 Ry was adopted to expand the valence wave functions and deficit charge density, respectively. The above cutoff energies give enough convergence in the relative energy of carbon-related materials within 1 meV/atom. Self-consistent electronic structure calculations were conducted with $4 \times 4 \times 1 \vec{k}$ -meshes for corannulene-intercalated bilayer graphene, where the corannulene molecules are sandwiched between graphene layers with 5×5 lateral periodicity. This choice of Brillouin zone integration corre-

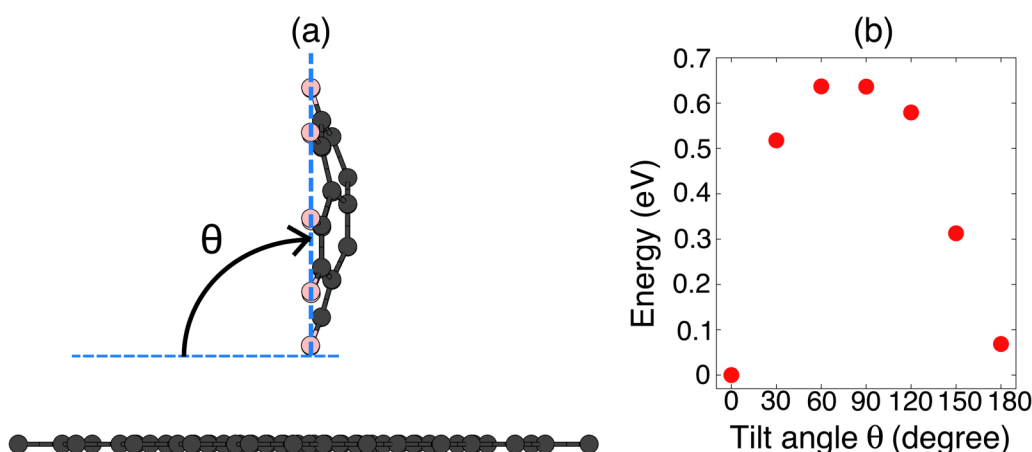


FIG. 1. (a) Geometric structure of corannulene on graphene with tilt angle $\theta = 90^\circ$. The black and pink balls denote C and H atoms, respectively. (b) Relative total energy of corannulene on a graphene layer as a function of tilt angle θ . Energy is measured from that of the ground state ($\theta = 0^\circ$).

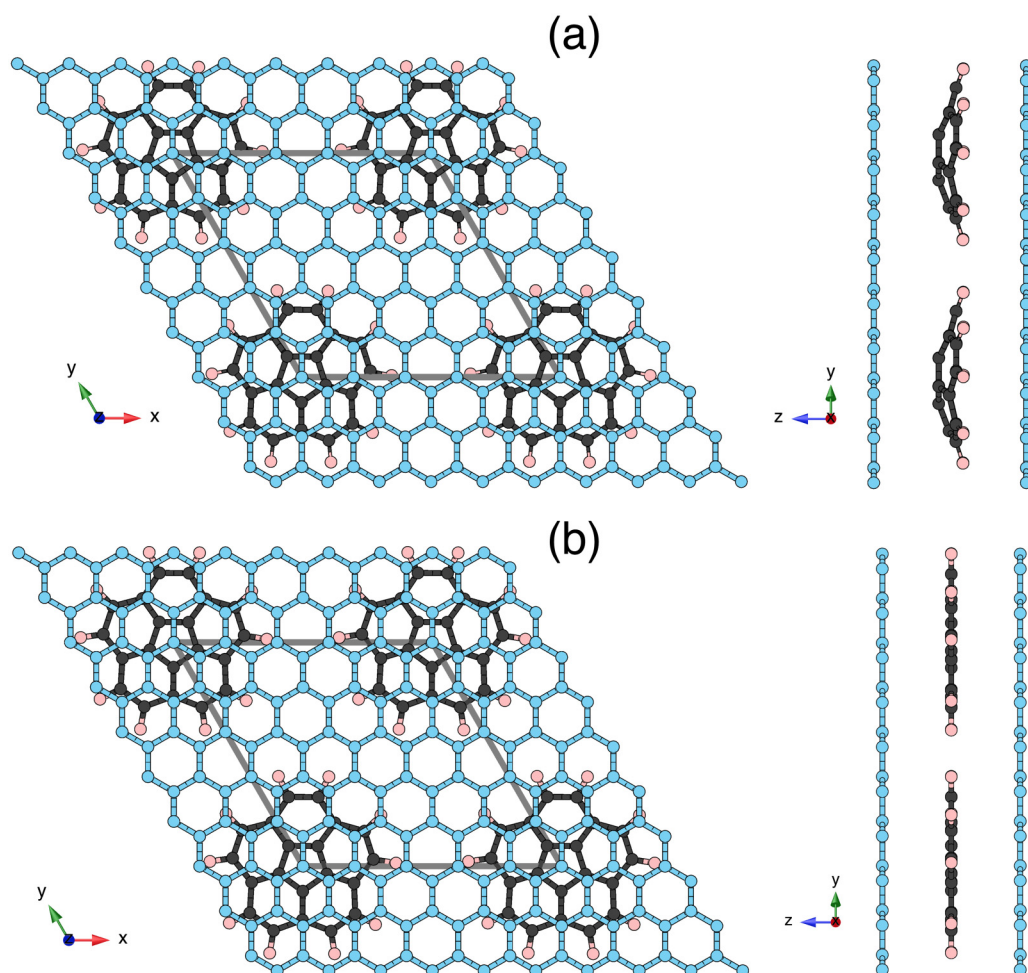


FIG. 2. Top and side views of optimized geometric structures of bilayer graphene with AA stacking arrangement intercalating corannulene with (a) bowl and (b) flat conformations. The black, pink, and blue circles indicate C atoms of corannulene, H atoms of corannulene, and C atoms of graphene, respectively. The gray parallelograms denote the lateral super cell of corannulene-intercalated bilayer graphene corresponding to 5×5 lateral periodicity of graphene.

sponds to the $20 \times 20 \times 1 \vec{k}$ -meshes in a conventional unit cell of graphene, which gives sufficient convergence in the total energy and electronic structure of graphene and its derivatives. Structural optimization was carried out until the remaining forces on each atom were less than $5 \text{ mRy}/\text{\AA}$. Because an intrinsic dipole moment normal to the molecular plane of corannulene is expected, we adopted the effective screening medium method (ESM) to avoid an unphysical interaction between dipoles in imaging cells normal to the corannulene-intercalated bilayer graphene, separated by a vacuum spacing of at least 10 \AA , under a conventional plane-wave DFT code.⁵⁸ In the ESM, we adopted an open boundary condition with respect to the electrostatic properties normal to the graphene layers by considering the generalized Poisson equation with a relative permittivity of 1 for all systems and a vanishing potential gradient at the cell boundaries.

III. RESULTS AND DISCUSSION

Before considering corannulene-intercalated bilayer graphene, we investigated the molecular arrangement of corannulene on a graphene layer because corannulene can possess several arrangements with respect to the graphene sheet. Figure 1 shows the relative energy of corannulene on graphene as a function of the tilt angle of the molecular plane with respect to the graphene layer. Corannulene has two stable molecular arrangements with respect to the tilt angle. A corannulene molecule favors arrangements where either its edge H atoms are on the graphene side ($\theta = 0^\circ$) or the convex region is on the graphene side ($\theta = 180^\circ$). Among these two arrangements, $\theta = 0^\circ$ is the ground state, with an energy 69 meV lower than that of $\theta = 180^\circ$. The energy monotonically increases with increasing or decreasing tilt angle from $\theta = 0^\circ$ or $\theta = 180^\circ$, respectively, and has a peak around $\theta = 90^\circ$, where

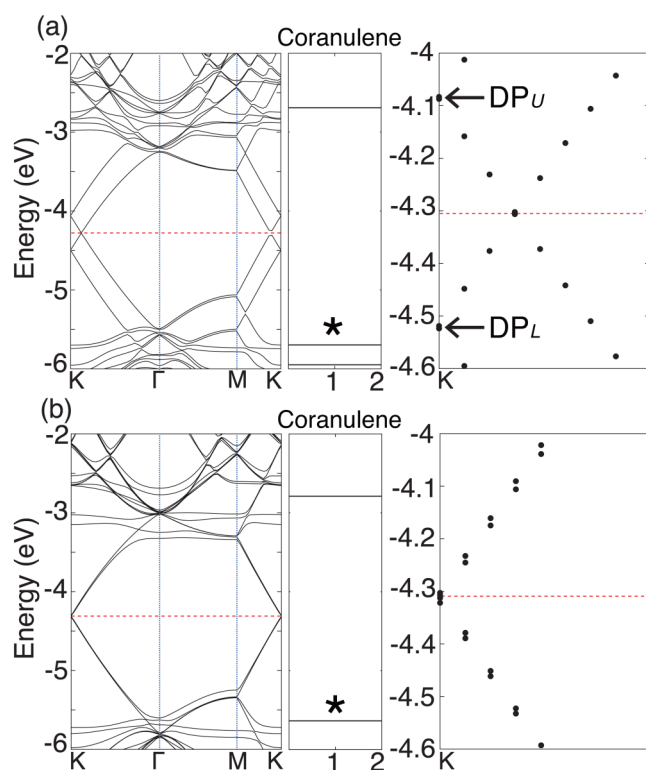


FIG. 3. Electronic band structures of corannulene-intercalated bilayer graphene with (a) bowl and (b) flat conformations. The vertical blue and horizontal red dotted lines denote the symmetric points in reciprocal space and the Fermi level, respectively. Electronic structures of an isolated corannulene molecule with bowl and flat conformations are also shown in the middle panel of each figure. The degeneracy labels 1 and 2 indicate the non-degenerated and doubly degenerated states, respectively. Asterisks denote the highest occupied states of an isolated corannulene. Enlarged band structures near the Fermi level and the K point are shown in the right panel in each figure. Labels DP_U and DP_L indicate the upper and lower Dirac points split by the intercalation of corannulene with bowl conformation. Energy is measured from that of the vacuum level.

corannulene has a standing arrangement as it does in carbon nanotubes.⁴⁷ The asymmetric energy profile with respect to the tilt angle is due to its bowl shape. The energy measured from the ground state increases because the $CH-\pi$ interaction decreases with increasing tilt angle. The decrease in energy from the peak is due to the increase in $\pi-\pi$ interaction between corannulene and graphene. This implies that corannulene molecules form a two-dimensional membrane structure on graphene.

Figure 2 shows optimized geometries of corannulene-intercalated bilayer graphene where corannulene has bowl and flat conformations. These complexes with different molecular conformations have approximately the same total energy, but the bowl conformation is more stable than the flat by 65 meV/molecule. This energy difference is substantially smaller than that of isolated corannulene, where the transition energy of the flat conformation is 434 meV/molecule higher than that of the ground state bowl conformation. Therefore,

the nanoscale spacing in bilayer graphene realizes flat conformation of corannulene under adequate conditions in addition to the bowl shape ground state conformation. The small energy difference between the bowl and flat conformations of corannulene may also cause a quick bowl-inversion reaction inside the confined space of bilayer graphene.⁵⁹ The bowl-inversion reaction probability in nanoscale spacing substantially increases compared with that in the vacuum by thousand and million times under the temperatures of 500 and 300 K, respectively. The optimum spacing between the convex part or H atom on the edge of corannulene and the graphene layers is 3.0 Å for the bowl conformation, whereas the spacing between corannulene with flat conformation and a graphene layer is 3.3 Å. Note that corannulene intercalated in bilayer graphene with 5×5 lateral periodicity is separated from its six adjacent molecules by 3.8 and 3.4 Å in the bowl and flat molecular conformations, respectively.

Figures 3(a) and 3(b) show the electronic structures of corannulene-intercalated bilayer graphene with bowl and flat conformations, respectively. The bilayer graphene intercalating corannulene with bowl structure is a metal possessing Dirac cones around the Fermi level. Interestingly, the two Dirac cones are split into upper and lower cones with an energy difference of 0.44 eV at the K point [Fig. 3(a)]. This splitting may enable electron transfer from the upper Dirac cone to the lower one, leading to electron and hole redistribution in a bilayer graphene intercalation compound consisting of carbon atoms. The calculated electron and hole densities of the lower and upper Dirac bands are each $5.3 \times 10^{12}/\text{cm}^2$, estimated by integrating the electron and hole densities injected into these bands. Note that the carrier density is comparable to that realized in conventional field effect transistors. The energy bands associated with the highest occupied and lowest unoccupied states of corannulene emerge 1 eV above and 1.5 eV below the upper Dirac point (DP_U) and lower Dirac point (DP_L), respectively. Furthermore, each of these states loses its twofold degeneracy and is highly modulated when the states cross the dispersive energy bands associated with graphene. These facts imply that the electronic states of corannulene highly affect the electronic properties of graphene. Indeed, the upper and lower Dirac cones have tiny energy gaps of 4.0 and 4.7 meV at the K point owing to orbital hybridization between corannulene and graphene.

In contrast, corannulene-intercalated bilayer graphene with a flat conformation approximately retains the characteristic electronic structures of bilayer graphene with large interlayer spacing. Two Dirac cones emerge at the Fermi level, indicating that charge transfer is absent [Fig. 3(b)]. By carefully checking the energy band at the Fermi level, these Dirac bands are no longer degenerate with each other but are split into four individual states with a gap of approximately 4.7–9.3 meV. This electronic band structure modulation also implies that the interaction between graphene and corannulene is crucial in determining the electronic properties of this complex, irrespective of the molecular conformation in bilayer graphene.

To investigate the physical origin of the Dirac cone splitting, we investigated the wave function distribution of Kohn–Sham orbitals of the Dirac bands of corannulene-intercalated bilayer graphene (Fig. 4). For the bilayer graphene intercalating bowl conformation, the wave functions of the upper and lower Dirac points are distributed in layers at the convex and H-terminated edge sides of

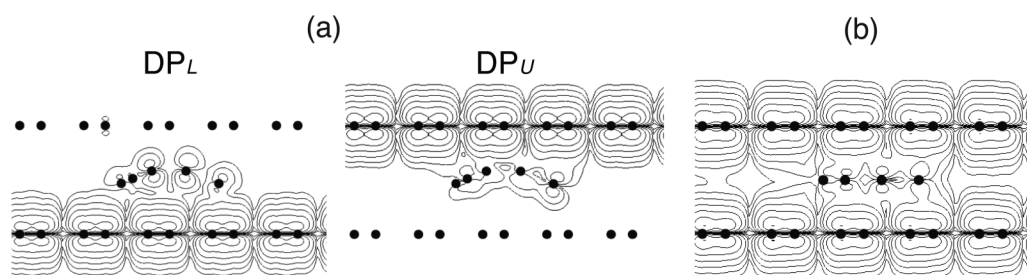


FIG. 4. (a) Isosurfaces of the squared wave function of Kohn-Sham orbitals of lower Dirac point (DP_L) and upper Dirac point (DP_U) at the K point of corannulene-intercalated bilayer graphene with bowl conformation. The labels correspond to those in Fig. 3. (b) Isosurfaces of the squared wave function of Kohn-Sham orbitals of the valence and conduction band edges at the K point of corannulene-intercalated bilayer graphene with flat conformation.

corannulene, respectively, both with π state nature similar to that of an isolated graphene layer [Fig. 4(a)]. This result confirms that holes and electrons are injected into the graphene layers at the convex and edge sides, respectively. In addition, a substantial wave function distribution is found on corannulene for both states. Thus, the orbital hybridization between graphene layers and corannulene is crucial in this material. For the corannulene-intercalated bilayer graphene with flat conformation, the wave functions of the valence band edge and the conduction band edge are distributed over both graphene and corannulene with π state nature [Fig. 4(b)], indicating that the substantial interaction between graphene and corannulene affects the electronic structure modulation of graphene.

The Dirac cone splitting of 0.44 eV suggests that the electron and hole redistribution in the bilayer graphene is due to the dipole moment of corannulene sandwiched between graphene layers. To clarify the physical origin of the charge transfer between the top and bottom graphene layers, we investigated the electrostatic potential of corannulene-intercalated bilayer graphene with a bowl conformation [Fig. 5(a)]. The electrostatic potential of the top vacuum is 0.45 V higher than that of the bottom vacuum, which is approximately the same as the Dirac cone splitting. According to this potential difference, electrons are transferred from the top graphene layer to the bottom one, resulting in holes residing in the top layer and electrons in the bottom layer. The potential difference between the upper and lower graphene layers implies the dipole moment of corannulene sandwiched between them. Therefore, the molecular dipole moment is the physical origin of the induced charge transfer between the graphene layers owing to the electrostatic potential difference between them. Notably, the convex region of corannulene has a higher potential profile than that induced by the C-H polarization at the edge atomic sites. There is obviously no potential difference between graphene layers for corannulene with flat conformation [Fig. 5(b)]. The electrostatic potential is symmetric with respect to the middle of the upper and lower graphene layers.

Electron and hole redistribution in bilayer graphene intercalated corannulene suggests the possibility of all carbon p-n border at an interface between corannulene with convex and concave arrangements. To assess the possibility, we consider the superlattice consisting of strips of bilayer graphene with 20×5 supercell where corannulene is alternately arranged in convex and concave with

quadruple periodicity [Fig. 6(a)]. Figure 6(b) shows the projected density of states (pDOS) of corannulene-intercalated bilayer graphene on C atoms belonging to upper and lower layers. Dirac points on upper and lower graphene layers strongly depend on the molecular arrangement of corannulene: the Dirac point on the upper graphene layer shifts downward, while that on the lower graphene shifts upward with increasing x coordinate. Accordingly, the Dirac bands belonging to the upper and lower graphene layers intersect each other owing to the polarity change at the interface between corannulene with convex and concave arrangements in bilayer graphene [Fig. 6(c)]. Therefore, p-n and n-p borders realized on upper and lower graphene layers, respectively, at the interface between convex and concave molecular arrangement [$x \sim 17$ Å in Fig. 6(b)], indicating that the corannulene-intercalated bilayer graphene is the possible all carbon p-n border whose polarity is tunable by controlling molecular arrangement and conformation.

The Dirac point bending with respect to the atomic position on upper and lower graphene layers is corroborated by the electrostatic potential on graphene layers. Figure 7 shows color plots of electrostatic potential on upper and lower graphene layers which sandwich corannulene membrane. Electrostatic potential on upper graphene around the convex region is shallower than that around the concave region. In contrast, electrostatic potential on lower

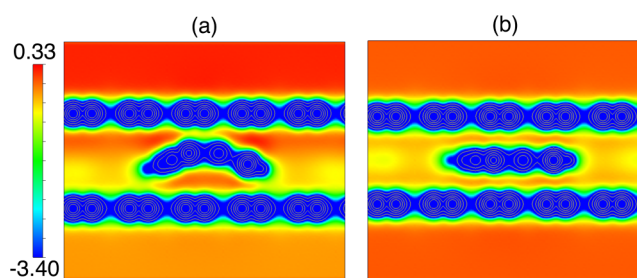


FIG. 5. Contour plots of the electrostatic potential of corannulene-intercalated bilayer graphene with (a) bowl and (b) flat conformations on the plane normal to the graphene layers and corannulene. The red and blue regions indicate the regions of high and low electrostatic potential, respectively. Each contour line represents double (or half) the density of the adjacent contour lines.

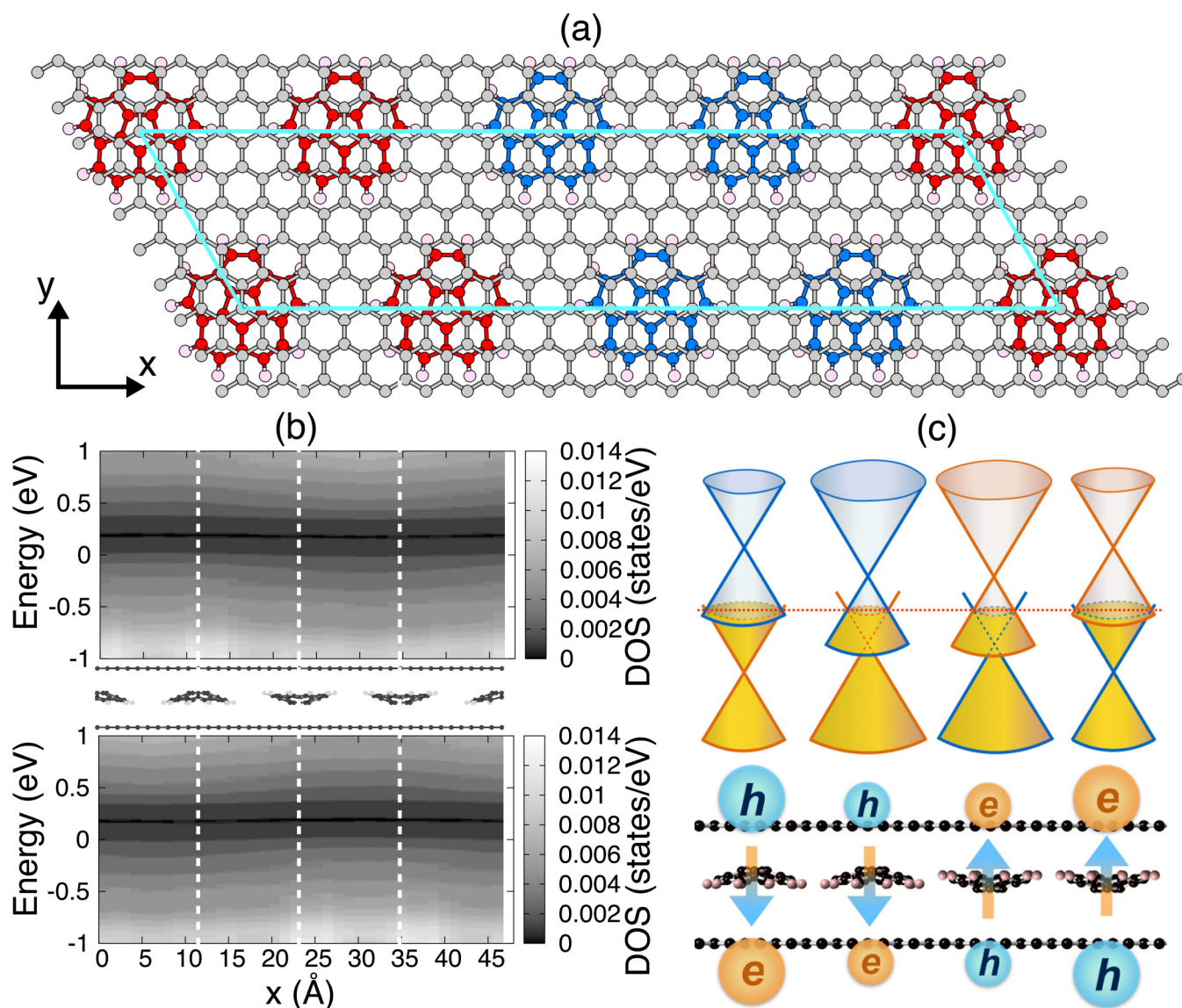


FIG. 6. (a) A geometric structure of superlattice consisting of strips of bilayer graphene with 20×5 supercell where corannulene is alternately arranged in convex and concave with quadruple periodicity. Red, blue, gray, and pink balls denote C atoms of corannulene molecule with convex arrangement, C atoms of corannulene molecule with concave arrangement, C atoms of bilayer graphene, and H atoms, respectively. Right blue lines indicate a unit cell. (b) Projected density of states (pDOS) of corannulene-intercalated bilayer graphene on C atoms belonging to the upper layer (the upper panel) and lower layer (the lower panel). Vertical dotted lines indicate the corannulene position. A corresponding side view of the geometric structure of corannulene-intercalated bilayer graphene is given in the middle panel. (c) A schematic band diagram associated with the Dirac points near the interface between corannulene with convex and concave arrangements in bilayer graphene. Blue and red cones correspond with the Dirac cones belonging to upper and lower graphene layers, respectively. Arrows indicate the direction of polarity of corannulene.

graphene around the convex region is deeper than that around the concave region. The estimated potential difference on the graphene layer between convex and concave regions is approximately 0.16 V. This value is smaller than that obtained in bilayer graphene encapsulating corannulene that is unidirectionally aligned because of the small width of concave and convex regions.

Molecular conformation and arrangement crucially affect the electronic properties of bilayer graphene. Applying pressure is one plausible way to achieve flat molecular conformation of corannulene between graphene layers. Figure 8 shows the calculated total energy of bilayer graphene intercalating corannulene with bowl and flat conformations as a function of interlayer spacing. The energy

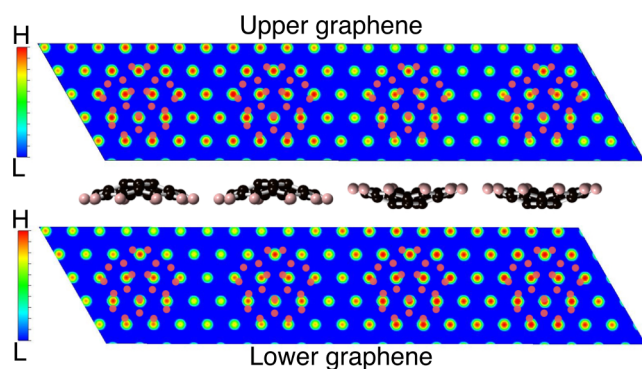


FIG. 7. Color plot of the electrostatic potential of corannulene-intercalated bilayer graphene around upper graphene (the upper panel) and lower graphene (the lower panel). Orange dots denote the position of C atoms in corannulene projected to the graphene layers. The red and blue regions indicate the regions of high and low electrostatic potential, respectively. Lateral corannulene arrangements are depicted in the middle panel. Black and pink balls denote C and H atoms, respectively.

profile suggests the possibility of a structural transformation of corannulene from bowl to flat conformations between the graphene layers. The free energy of the system is expressed as $F = U - TS$, where U corresponds to the calculated total energy, S is the entropy, and T is the temperature. We can use this to discuss the

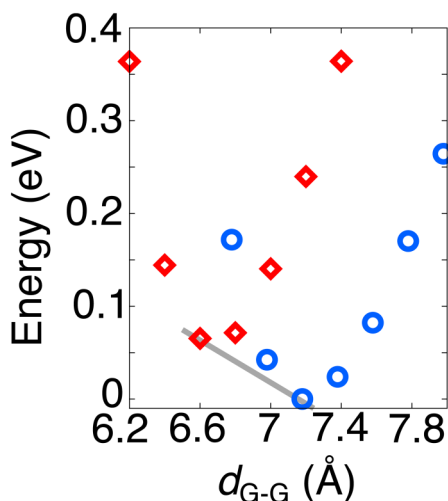


FIG. 8. Calculated relative total energy of corannulene-intercalated bilayer graphene as a function of interlayer spacing of bilayer graphene, d_{G-G} . The blue circles and red rhombuses indicate the energies of corannulene-intercalated bilayer graphene with bowl and flat conformations, respectively. Energies are measured from the ground state of corannulene-intercalated bilayer graphene with the bowl conformation. The gray line is a common tangent between the two energy curves of corannulene-intercalated bilayer graphene with bowl and flat conformations.

pressure-inducing phase transition on the complex under 0 K using the energy curves in Fig. 8. The fitting curves in Fig. 8 are obtained through polynomial fitting up to the fifth order of z . The common tangential line for both energy curves is then calculated from $P = \frac{1}{S_{uc}} \frac{\partial F}{\partial z} = \frac{1}{S_{uc}} \frac{\partial U}{\partial z}$, where S_{uc} is the area of the unit cell. We can conclude that the intercalated corannulene undergoes a structural phase transition from bowl to flat molecular conformations under a critical pressure of $P_c = 139$ MPa. Notably, flipping motion of corannulene increases with increasing temperature (Fig. S1 in the supplementary material) so that the critical pressure decreases with increasing temperature. Thus, corannulene with flat conformation can be obtained by applying external pressure, and it retains its conformation under the pressure. In addition to the pressure, an external electric field normal to the molecular plane may also control the molecular conformation (Fig. S2 in the supplementary material).

IV. CONCLUSION

On the basis of DFT with the generalized gradient approximation, we theoretically investigated the geometric and electronic structures of a carbon-based intercalation compound comprising bilayer graphene and a bowl-shaped hydrocarbon corannulene, as the thinnest potential graphite intercalation compound. Corannulene favors a lying molecular arrangement with respect to the graphene layer, so it forms a potential molecular layer on graphene or between graphene layers. Intercalation of corannulene into bilayer graphene decreases the energy difference between the bowl and flat conformations of corannulene, so corannulene has a flat conformation in the interlayer spacing of bilayer graphene under a uniaxial pressure of 139 MPa. Furthermore, a rapid bowl-inversion reaction is expected to occur under room temperature. The dipole moment normal to the molecular plane of corannulene causes an electrostatic potential difference between graphene layers when bowl-shaped corannulene is intercalated into the interlayer spacing of bilayer graphene. The Dirac cones split into upper and lower cones reflecting the potential difference between the graphene layers such that the splitting induces opposing carriers in the layers. Hole and electron densities, each $5.3 \times 10^{12}/\text{cm}^2$, are induced on the graphene layers situated at the convex and edge sides of intercalated corannulene, respectively. Substantial orbital hybridization between graphene layers and corannulene causes substantial modulation in the electronic states of each constituent unit. Electron and hole redistribution in bilayer graphene intercalating corannulene indicated the possibility of all carbon p-n border at an interface between corannulene with convex and concave arrangements.

SUPPLEMENTARY MATERIAL

See the supplementary material for the geometric structure of bilayer graphene intercalated corannulene under the temperature 300 K, using *ab initio* molecular dynamics simulation, and a bowl inversion of an isolated corannulene under the external electric field.

ACKNOWLEDGMENTS

This work was supported by the Japan Science and Technology Agency (JST-CREST) (Grant Nos. JPMJCR20B5 and

JPMJCR1715), the Japan Society for the Promotion of Science (JSPS KAKENHI) (Grant Nos. JP21H05233, JP21H05232, JP21K14484, JP20H05664, JP20K05253, JP20H02080, and JP20H00316), the Joint Research Program on Zero-Emission Energy Research of the Institute of Advanced Energy at Kyoto University, and the University of Tsukuba Basic Research Support Program (S). Part of the calculations was performed on an NEC SX-Ace at the Cybermedia Center, Osaka University.

AUTHOR DECLARATIONS

Conflict of Interest

The authors have no conflicts to disclose.

DATA AVAILABILITY

The data that support the findings of this study are available from the corresponding author upon reasonable request.

REFERENCES

- ¹R. C. Tatar and S. Rabi, "Electronic properties of graphite: A unified theoretical study," *Phys. Rev. B* **25**, 4126 (1982).
- ²M. S. Dresselhaus and G. Dresselhaus, "Intercalation compounds of graphite," *Adv. Phys.* **30**, 139 (2006).
- ³K. S. Novoselov, A. K. Geim, S. V. Morozov, D. Jiang, Y. Zhang, S. V. Dubonos, I. V. Grigorieva, and A. A. Firsov, "Electric field effect in atomically thin carbon films," *Science* **306**, 666 (2004).
- ⁴C. Lee, X. Wei, J. W. Kysar, and J. Hone, "Measurement of the elastic properties and intrinsic strength of monolayer graphene," *Science* **321**, 385 (2008).
- ⁵J. H. Seol *et al.*, "Two-dimensional phonon transport in supported graphene," *Science* **328**, 213 (2010).
- ⁶X. Du, I. Skachko, A. Barker, and E. Y. Andrei, "Approaching ballistic transport in suspended graphene," *Nat. Nanotechnol.* **3**, 491 (2008).
- ⁷K. S. Novoselov, A. K. Geim, S. V. Morozov, D. Jiang, M. I. Katsnelson, I. V. Grigorieva, S. V. Dubonos, and A. A. Firsov, "Two-dimensional gas of massless Dirac fermions in graphene," *Nature* **438**, 197 (2005).
- ⁸Y. Zhang, Y.-W. Tan, H. L. Stormer, and P. Kim, "Experimental observation of the quantum Hall effect and Berry's phase in graphene," *Nature* **438**, 201 (2005).
- ⁹X. Du, I. Skachko, F. Duerr, A. Luican, and E. Y. Andrei, "Fractional quantum Hall effect and insulating phase of Dirac electrons in graphene," *Nature* **462**, 192 (2009).
- ¹⁰K. I. Bolotin, F. Ghahari, M. D. Shulman, H. L. Stormer, and P. Kim, "Observation of the fractional quantum Hall effect in graphene," *Nature* **462**, 196 (2009).
- ¹¹M. Fujita, K. Wakabayashi, K. Nakada, and K. Kusakabe, "Peculiar localized state at zigzag graphite edge," *J. Phys. Soc. Jpn.* **65**, 1920 (1996).
- ¹²N. Shima and H. Aoki, "Electronic structure of super-honeycomb systems: A peculiar realization of semimetal/semiconductor classes and ferromagnetism," *Phys. Rev. Lett.* **71**, 4389 (1993).
- ¹³M. Maruyama, N. T. Cuong, and S. Okada, "Coexistence of Dirac cones and Kagome flat bands in a porous graphene," *Carbon* **109**, 755 (2016).
- ¹⁴M. Maruyama and S. Okada, "Interplay between the Kagome flat band and the Dirac cone in porous graphitic networks," *Carbon* **125**, 530 (2017).
- ¹⁵S. Masubuchi, M. Morimoto, S. Morikawa, M. Onodera, Y. Asakawa, K. Watanabe, T. Taniguchi, and T. Machida, "Autonomous robotic searching and assembly of two-dimensional crystals to build van der Waals superlattices," *Nat. Commun.* **9**, 722 (2018).
- ¹⁶S. Masubuchi, E. Watanabe, Y. Seo, S. Okazaki, T. Sasawaga, K. Watanabe, T. Taniguchi, and T. Machida, "Deep-learning-based image segmentation integrated with optical microscopy for automatically searching for two-dimensional materials," *npj 2D Mater. Appl.* **4**, 2481 (2020).
- ¹⁷M. Onodera, S. Masubuchi, R. Moriya, and T. Machida, "Assembly of van der Waals heterostructures: Exfoliation, searching, and stacking of 2D materials," *Jpn. J. Appl. Phys.* **59**, 010101 (2020).
- ¹⁸R. Ribeiro-Palau, C. Zhang, K. Watanabe, T. Taniguchi, J. Hone, and C. R. Dean, "Twistable electronics with dynamically rotatable heterostructures," *Science* **361**, 690 (2018).
- ¹⁹M. Koshino and E. McCann, "Trigonal warping and Berry's phase $N\pi$ in ABC-stacked multilayer graphene," *Phys. Rev. B* **80**, 165409 (2009).
- ²⁰M. Koshino, "Interlayer screening effect in graphene multilayers with ABA and ABC stacking," *Phys. Rev. B* **81**, 125304 (2010).
- ²¹M. Otani, Y. Takagi, M. Koshino, and S. Okada, "Phase control of magnetic state of graphite thin films by electric field," *Appl. Phys. Lett.* **96**, 242504 (2010).
- ²²M. Otani, M. Koshino, Y. Takagi, and S. Okada, "Intrinsic magnetic moment on (0001) surfaces of rhombohedral graphite," *Phys. Rev. B* **81**, 161403(R) (2010).
- ²³Y. Cao, V. Fatemi, S. Fang, K. Watanabe, T. Taniguchi, E. Kaxiras, and P. Jarillo-Herrero, "Unconventional superconductivity in magic-angle graphene superlattices," *Nature* **556**, 43 (2018).
- ²⁴T. Enoki, M. Suzuki, and M. Endo, *Graphite Intercalation Compounds and Applications* (Oxford University Press, New York, 2003).
- ²⁵A. Koma, K. Miki, H. Suematsu, T. Ohno, and H. Kamimura, "Density-of-states investigation of C_8K and occurrence of the interlayer band," *Phys. Rev. B* **34**, 2434 (1986).
- ²⁶G. S. Parry and D. E. Nixon, "Order-disorder transformation in potassium graphite," *Nature* **216**, 909 (1967).
- ²⁷A. Metrot, D. Guerd, D. Bikkaud, and A. Herold, "New results about the sodium-graphite system," *Synth. Met.* **1**, 363 (1980).
- ²⁸T. E. Weller, M. Ellerby, S. S. Saxena, R. P. Smith, and N. T. Skipper, "Superconductivity in the intercalated graphite compounds C_6Yb and C_6Ca ," *Nat. Phys.* **1**, 39 (2005).
- ²⁹M. Posternak, A. Baldereschi, A. J. Freeman, E. Wimmer, and M. Weinert, "Prediction of electronic interlayer states in graphite and reinterpretation of alkali bands in graphite intercalation compounds," *Phys. Rev. Lett.* **50**, 761 (1983).
- ³⁰M. Posternak, A. Baldereschi, A. J. Freeman, and E. Wimmer, "Prediction of electronic surface states in layered materials: Graphite," *Phys. Rev. Lett.* **52**, 863 (1984).
- ³¹H. Suematsu, K. Ohmatsu, T. Sakakibara, M. Date, and M. Suzuki, "Magnetic properties of europium-graphite intercalation compound C_6Eu ," *Synth. Met.* **8**, 23 (1983).
- ³²F. Beguin, R. Setton, L. Facchini, A. P. Legrand, G. Merle, and C. Mai, "Structure and properties of $KC_{24}(Bz)_2$, a graphite-potassium-benzene intercalation compound," *Synth. Met.* **2**, 161 (1980).
- ³³Yu. V. Isaev, Yu. N. Novikov, M. E. Vol'pin, I. Rashkov, and I. Panayotov, "Ternary lamellar graphite compounds with potassium and methylbenzenes," *Synth. Met.* **6**, 9 (1983).
- ³⁴J. Jegoudez, C. Mazieres, and R. Setton, "Behaviour of the binary graphite intercalation compounds KC_8 and KC_{24} towards a set of sample organic molecules," *Synth. Met.* **7**, 85 (1983).
- ³⁵S. Saito and A. Oshiyama, "Design of C_{60} -graphite cointercalation compounds," *Phys. Rev. B* **49**, 17413 (1994).
- ³⁶E. V. Rut'kov, A. Ya. Tontegode, and M. M. Usufov, "Evidence for a C_{60} monolayer intercalated between a graphite monolayer and iridium," *Phys. Rev. Lett.* **74**, 758 (1995).
- ³⁷V. Gupta, P. Scharff, K. Risch, H. Romanus, and R. Müller, "Synthesis of C_{60} intercalated graphite," *Solid State Commun.* **131**, 153 (2004).
- ³⁸H. Kinoshita, I. Jeon, M. Maruyama, K. Kawahara, Y. Terao, D. Ding, R. Matsumoto, Y. Matsuo, S. Okada, and H. Ago, "Highly conductive and transparent large-area bilayer graphene realized by $MoCl_5$ intercalation," *Adv. Mater.* **29**, 1702141 (2017).
- ³⁹K. Kanahashi *et al.*, "Formation of environmentally stable hole-doped graphene films with instantaneous and high-density carrier doping via a boron-based oxidant," *npj 2D Mater. Appl.* **3**, 7 (2019).

- ⁴⁰W. E. Barth and R. G. Lawton, "Dibenzo[ghi,mno]fluoranthene," *J. Am. Chem. Soc.* **88**, 380 (1966).
- ⁴¹A. M. Butterfield, B. Gilomen, and J. S. Siegel, "Kilogram-scale production of corannulene," *Org. Process Res. Dev.* **16**, 664 (2012).
- ⁴²S. Higashibayashi, R. Tsuruoka, Y. Soujanya, U. Purushotham, G. N. Sadry, S. Seki, T. Ishikawa, S. Toyota, and H. Sakurai, "Trimethylsumanene: Enantioselective synthesis, substituent effect on bowl structure, inversion energy, and electron conductivity," *Bull. Chem. Soc. Jpn.* **85**, 450 (2012).
- ⁴³M. Parschau, R. Fasel, K.-H. Ernst, O. Gröning, L. Brandenberger, R. Schillinger, T. Greber, A. Seitsonen, Y.-T. Wu, and J. Siegel, "Buckybowls on metal surfaces: Symmetry mismatch and enantiomorphism of corannulene on Cu(110)," *Angew. Chem. Int. Ed.* **46**, 8258 (2007).
- ⁴⁴R. Jaafar, C. A. Pignedoli, G. Bussi, K. Ait-Mansour, O. Groening, T. Amaya, T. Hirao, R. Fasel, and P. Ruffieux, "Bowl inversion of surface-adsorbed sumanene," *J. Am. Chem. Soc.* **136**, 13666 (2014).
- ⁴⁵S. Fujii, M. Ziatdinov, S. Higashibayashi, H. Sakurai, and M. Kiguchi, "Bowl inversion and electronic switching of buckybowls on gold," *J. Am. Chem. Soc.* **138**, 12142 (2016).
- ⁴⁶M. Maruyama and S. Okada, "Carrier redistribution in van der Waals nanostructures consisting of bilayer graphene and buckybowls: Implications for piezoelectric devices," *ACS Appl. Nano Mater.* **4**, 3007 (2021).
- ⁴⁷Y. Izumi, Z. Liu, K. Suenaga, S. Okada, S. Higashibayashi, H. Sakurai, and T. Okazaki, "Molecular arrangements of corannulene and sumanene in single-walled carbon nanotubes," *ChemNanoMat* **4**, 557 (2018).
- ⁴⁸P. Hohenberg and W. Kohn, "Inhomogeneous electron gas," *Phys. Rev.* **136**, B864 (1964).
- ⁴⁹W. Kohn and L. J. Sham, "Self-consistent equations including exchange and correlation effects," *Phys. Rev.* **140**, A1133 (1965).
- ⁵⁰Y. Morikawa, K. Iwata, and K. Terakura, "Theoretical study of hydrogenation process of formate on clean and Zn deposited Cu(111) surfaces," *Appl. Surf. Sci.* **169–170**, 11 (2001).
- ⁵¹See <https://state-doc.readthedocs.io/en/latest/index.html> for Simulation Tool for Atom TEchnology (STATE).
- ⁵²J. P. Perdew, K. Burke, and M. Ernzerhof, "Generalized gradient approximation made simple," *Phys. Rev. Lett.* **77**, 3865 (1996).
- ⁵³J. P. Perdew, K. Burke, and M. Ernzerhof, "Generalized gradient approximation made simple [Phys. Rev. Lett. **77**, 3865 (1996)]," *Phys. Rev. Lett.* **78**, 1396 (1997).
- ⁵⁴K. Lee, É. D. Murray, L. Kong, B. I. Lundqvist, and D. C. Langreth, "Higher-accuracy van der Waals density functional," *Phys. Rev. B* **82**, 081101(R) (2010).
- ⁵⁵V. R. Cooper, "Van der Waals density functional: An appropriate exchange functional," *Phys. Rev. B* **81**, 161104(R) (2010).
- ⁵⁶Y. Hamamoto, I. Hamada, K. Inagaki, and Y. Morikawa, "Self-consistent van der Waals density functional study of benzene adsorption on Si(100)," *Phys. Rev. B* **93**, 245440 (2016).
- ⁵⁷D. Vanderbilt, "Soft self-consistent pseudopotentials in a generalized eigenvalue formalism," *Phys. Rev. B* **41**, 7892 (1990).
- ⁵⁸M. Otani and O. Sugino, "First-principles calculations of charged surfaces and interfaces: A plane-wave nonrepeated slab approach," *Phys. Rev. B* **73**, 115407 (2006).
- ⁵⁹L. T. Scott, M. M. Hashemi, and M. S. Bratcher, "Corannulene bowl-to-bowl inversion is rapid at room temperature," *J. Am. Chem. Soc.* **114**, 1920 (1992).